Use of radially polarized beams in three-dimensional photonic crystal fabrication with the two-photon polymerization method

Baohua Jia,[1,2] Hong Kang,[1] Jiafang Li,[1] and Min Gu[1,*]

[1]*Centre for Micro-Photonics and Centre for Ultrahigh-Bandwidth Devices for Optical Systems (CUDOS),*
Faculty of Engineering and Industrial Sciences, Swinburne University of Technology, P.O. Box 218,
Hawthorn 3122, Australia
[2] *bjia@swin.edu.au*
**Corresponding author: mgu@swin.edu.au*

Radially polarized ultrafast laser beams are used in the fabrication of three-dimensional photonic crystals with the two-photon polymerization technique in organic–inorganic hybrid materials. It has been found that when a radially polarized beam is employed, the lateral size of the fabricated polymer rods is decreased by 27.5% from 138 to 100 nm under a threshold fabrication condition, leading to a 17.35% reduction in the filling ratio of the photonic crystal. A comparison of the stop gaps between radially polarized and linearly polarized beam illumination shows a higher suppression ratio in transmission and a wider wavelength range in the former case owing to the favorable tuning of the filling ratio of the three-dimensional photonic crystals. © 2009 Optical Society of America

OCIS codes: 220.4000, 050.6875, 050.5298.

Characterized by its unique polarization properties, a radially polarized beam, as shown in Figs. 1(a)–1(c), has attracted much attention in recent years [1–7]. The most intriguing property of a radially polarized beam is its highly symmetric and ultrasmall focal spot of the longitudinal component when being focused by a high-NA objective. Unlike the tight focusing of a linearly or circularly polarized beam, in which the depolarization induced longitudinal component deteriorates the overall focal spot by either splitting it into two lobes [8,9] or enlarging its size [10], the longitudinal component of a radially polarized beam is capable of dramatically increasing the lateral resolution of the overall focal spot when its strength is dominant. In particular, when such a beam is combined with other optical elements, for example, binary phase elements, which are specially designed to enhance the longitudinal component, even a "pure longitudinal needle" with lateral size beyond the diffraction limit can be created [5]. The capacity of achieving higher resolution has thus stimulated various exciting applications with radially polarized beams including linear and nonlinear microscopic imaging [1,2], optical laser trapping [4,11], and greatly enhanced surface plasmonic wave excitation [3,6]. In the meantime it also opens possible applications in optical data storage and optical lithography, in which resolution holds a key.

In this Letter, we demonstrate the use of radially polarized beams for the three-dimensional (3D) nanofabrication of 3D photonic crystals (PCs) with functional stop gaps using the two-photon polymerization (2PP) technique. It has been found that the lateral size of a single polymer rod in the fabricated PC can be greatly reduced by almost 40 nm compared with that fabricated with a linearly polarized beam under

the same threshold fabrication condition. In addition, owing to the highly symmetric nature of the focal spot, the resultant PC structures present better quality than those fabricated with linearly polarized beams.

Radially polarized beams can be generated by direct and indirect methods. With the direct method, radially polarized beams have been demonstrated as the output from the laser cavities [12,13]. With the indirect method, radial polarization has been produced by using spatial light modulators [1], interferometer [14,15], and segmented half-wave-plates [16]. In the current work the radially polarized beam is produced by a simple twisted nematic liquid crystal device (Arcoptix S.A.) operating in a broad wavelength region (400–1700 nm) [17]. High conversion efficiency of 75% can be experimentally achieved at 580 nm. As shown in Fig. 1(d), the radially polarized beam in free space shows a ring pattern that is similar to its theoretical counterpart [Fig. 1(a)]. An ex-
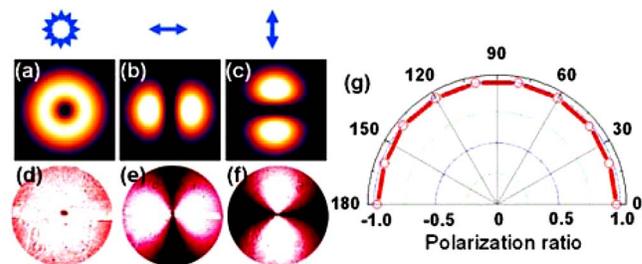

Fig. 1. (Color online) Simulated profiles of (a) a radially polarized beam and its (b) horizontal and (c) vertical polarization components before being focused by the fabrication objective. (d)–(f) Experimentally obtained profiles corresponding to (a)–(c), respectively. (d) The polarization ratio of the radially polarized beam in different polarization directions.

amination of the beam quality by an analyzer along the horizontal and vertical directions reveals two-lobe beam profiles [Figs. 1(e) and 1(f)], which reproduce the theoretical plots [Figs. 1(b) and 1(c)] demonstrating the high quality of the beam. The intensity distribution along every polarization direction is almost uniform (with an averaged change less than 5%), as shown in Fig. 1(g).

Such a radially polarized beam was launched into a standard 2PP fabrication system consisting of an ultrafast laser ($\lambda = 580$ nm, repetition rate$= 80$ MHz, pulse duration$= 200$ fs), a telescope based optical setup, a computer-controlled mechanical shutter, a high-precision 3D piezoscanning stage, and a high-NA (NA$= 1.4$) objective [18–21]. An organic–inorgnic hybrid resin Ormocer (refractive index $n \sim 1.47$) with a single-photon absorption band in the ultraviolet region was used in the fabrication. During the 2PP process a threshold fabrication method, which allows polymerization to occur at a minimum excitation laser power, was employed to reduce the fabricated feature size. The obtainable fabrication resolution was determined by the focal spot size of the objective and the response properties of the material.

To estimate the minimum achievable feature size, the two-photon intensity distributions of the focal spots of linearly and radially polarized beams are calculated through the coverglass ($n_1 = 1.515$) and polymer interface using the vectorial diffraction theory [22]. The results are shown in Figs. 2(a)–2(d). Owing to the significant contribution from the longitudinal component in the focal region [9,14,22], it is clearly seen that in the lateral plane, the linearly polarized beam shows an elongated focal spot along the incident polarization direction (the X axis). In comparison, the radially polarized beam presents a much symmetric profile with a reduced lateral size. In the axial direction (the Z axis), as expected, the radially polarized beam shows an extended focal size compared with that of the linearly polarized beam. A precise cross-section comparison of the focal spot along

both the lateral and axial directions is presented in Fig. 2(e). The FWHM of the lateral cross section in the linear polarization case is 228 nm. It is considerably reduced to 175 nm when a radially polarized beam is used, which leads to a 25% increase in the lateral resolution. In the mean time the axial resolution is degraded from 319 to 380 nm.

According to the calculated FWHM of the two-photon focal intensity distribution, the laser parameters used in the experiment and the two-photon absorption properties of the Ormocers [23], the diameter (D), and the length (L) of the achievable voxel can be predicted by employing simple equations described in [23]. In Fig. 3, the voxel diameter and length are calculated as functions of the input laser power for a constant exposure time of 5 ms. The experimentally obtained voxel size is also plotted in the same figure, which presents a perfect match with the calculated curve. It can be clearly seen that the diameter of the voxel can be decreased by more than 24% if a radial beam is used and the length of the voxel is increased by approximately 19%. In particular, in our experiment when a threshold fabrication power of 1.25 mW was used, the measured voxel diameter is 100 nm, which is 27.5% smaller than that (138 nm) fabricated under the linear polarization illumination with the same laser power. On the other hand, owing to an extended focus of the radially polarized beam, the length of a voxel is enlarged from 321 to 365 nm leading to a 14% increase.

The radially polarized beam was employed to fabricate 3D woodpile PCs. The fabrication results are presented in Fig. 4. In Fig. 4(a) the geometry of a woodpile PC is illustrated. Normally a woodpile PC follows a face-centered tetragonal (fct) geometry. But when $c/d = \sqrt{2}$ it becomes a face-centered cubic (fcc) crystal. In the current work, we focused on the fcc
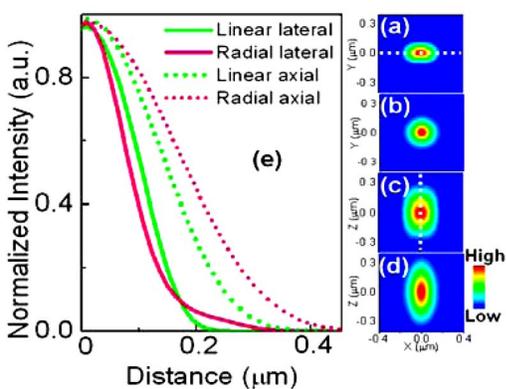
Fig. 2.   (Color online) Calculated two-photon intensity distributions along (a),(b) the transverse and (c),(d) the axial directions in the focal region of an objective with NA$= 1.4$ through the coverglass ($n_1 = 1.515$) and Ormocer ($n = 1.47$) interface under (a),(c) linearly polarized beam illumination and (b),(d) radially polarized beam illumination. (e) The cross section comparison of the focal spots along the X and the Z directions.
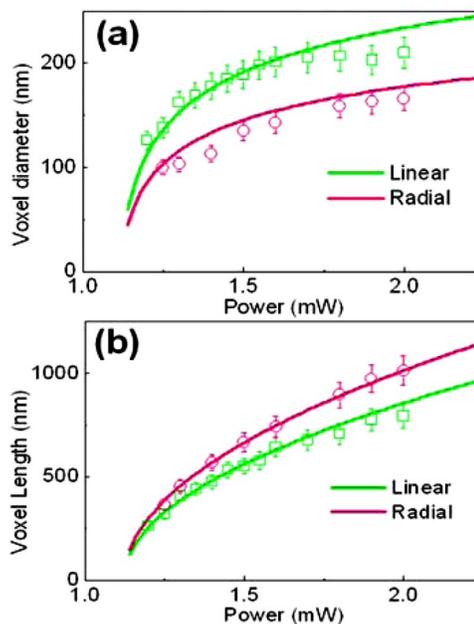
Fig. 3.   (Color online) Predicted (solid curve) and measured (dots and squares) (a) voxel diameter and (b) voxel length as functions of the laser power for a constant exposure time of $t = 5$ ms.
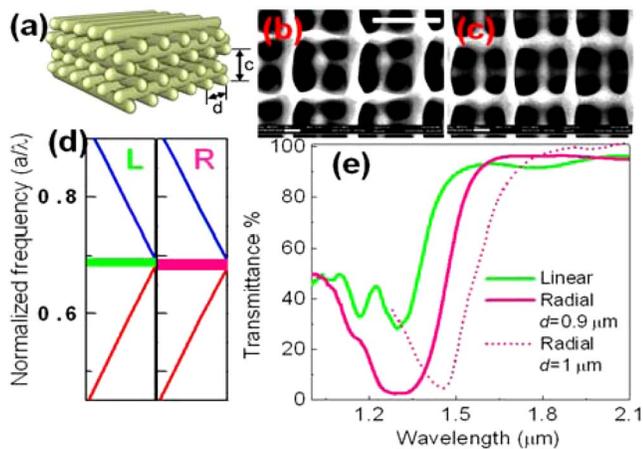
Fig. 4. (Color online) (a) Schematic of the woodpile PC. (b), (c) SEM images of PCs fabricated with (b) the linearly and (c) radially polarized beam illumination. Scale bar: 900 nm. (d) Calculated band diagrams in the Γ-X direction of structures in (b) and (c). (e) FTIR measured transmission spectra (solid curves) of PCs in (b) and (c) and another PC with different lattice constant ($d = 0.95$ μm) fabricated with a radially polarized beam.

structure. In Figs. 4(b) and 4(c), the scanning electron microscopic (SEM) images of the woodpile PCs fabricated with linearly and radially polarized beams under the same fabrication conditions (laser power $= 1.25$ mW, scanning speed$= 60$ μm/s, in-plane lattice constant$= 900$ nm) are presented, respectively. It can be clearly seen that the structure fabricated with a radially polarized beam shows thinner rods and a more symmetric overall structure. The rod thickness in Fig. 4(c) is less than 110 nm. Based on the fabrication results in Figs. 4(b) and 4(c), the band diagrams have been calculated using the MPB software [24], as shown in Fig. 4(d). In the Γ-X direction (i.e., the stacking direction of the woodpile), a stop gap starting from a normalized frequency of 0.68 is presenting in the PC fabricated with a linearly polarized beam. In comparison the stop gap shifted slightly toward the lower frequency region in the PC fabricated with a radially polarized beam because of the increase in the rod thickness in the stacking direction. In addition, owing to a favorable tuning of the filling ratio (17.35% reduction) of the woodpile, the stop gap exhibits a slightly wider frequency range compared with that fabricated with a linearly polarized beam.

The transmission spectra of the PCs measured with a Fourier-transform infrared (FTIR) spectrometer (Thermo Nicolet) in the Γ-X direction are displayed in Fig. 4(e). Stop gaps centered at a wavelength of 1.3 μm (corresponding to a normalized frequency of 0.69) have been observed in both cases, which agree well with the theoretically predicted gap position. It should be emphasized that the measured stop gap of the PC fabricated with a radially polarized beam shows a much higher transmission suppression ($>95\%$ versus $\sim60\%$) and a much wider wavelength region than those of the PC fabricated with a linearly polarized beam. The high quality stop

gap has also been consistently obtained when changing the lattice constant of the PC to $d = 0.95$ μm, as shown as the dotted curve in Fig. 4(e).

In conclusion, radially polarized beams have been utilized in the 2PP method to fabricate 3D PCs. Owing to the dominant contribution from the longitudinal component under the radially polarized beam illumination, the lateral fabrication resolution has been improved by more than 27.5%. As a result of this feature and the highly symmetric nature of the focal spot, the resultant PC structures present wider stop gaps with stronger suppression than those fabricated with linearly polarized beams.

References

1. E. Y. S. Yew and C. J. R. Sheppard, Opt. Commun. **275**, 453 (2007).
2. Y. Kozawa and S. Sato, J. Opt. Soc. Am. B **25**, 175 (2008).
3. K. J. Moh, X. C. Yuan, J. Bu, S. W. Zhu, and B. Z. Gao, Opt. Express **16**, 20734 (2008).
4. T. A. Nieminen, N. R. Heckenberg, and H. Rubinsztein-Dunlop, Opt. Lett. **33**, 122 (2008).
5. H. Wang, L. Shi, B. Lukyanchuk, C. Sheppard, and C. T. Chong, Nature Photon. **2**, 501 (2008).
6. N. M. Mojarad and M. Agio, Opt. Express **17**, 117 (2009).
7. R. Dorn, S. Quabis, and G. Leuchs, Phys. Rev. Lett. **91**, 233901 (2003).
8. M. Gu, J. B. Haumonte, Y. Micheau, J. W. M. Chon, and X. Gan, Appl. Phys. Lett. **84**, 4236 (2004).
9. B. Jia, X. Gan, and M. Gu, Appl. Phys. Lett. **86**, 131110 (2005).
10. G. M. Lerman and U. Levy, Opt. Express **16**, 4567 (2008).
11. Q. Zhan, Opt. Express **12**, 3377 (2004).
12. M. Fridman, G. MacHavariani, N. Davidson, and A. A. Friesem, Appl. Phys. Lett. **93**, 191104 (2008).
13. H. Kawauchi, Y. Kozawa, and S. Sato, Opt. Lett. **33**, 1984 (2008).
14. B. Jia, X. Gan, and M. Gu, Opt. Express **13**, 6821 (2005).
15. K. C. Toussaint, Jr., S. Park, J. E. Jureller, and N. F. Scherer, Opt. Lett. **30**, 2846 (2005).
16. H. Kawauchi, Y. Kozawa, S. Sato, T. Sato, and S. Kawakami, Opt. Lett. **33**, 399 (2008).
17. M. Stalder and M. Schadt, Opt. Lett. **21**, 1948 (1996).
18. S. Wu, J. Serbin, and M. Gu, J. Photochem. Photobiol., A **181**, 1 (2006).
19. J. Serbin and M. Gu, Adv. Mater. **18**, 221 (2006).
20. M. Straub and M. Gu, Opt. Lett. **27**, 1824 (2002).
21. B. Jia, J. Li, and M. Gu, Aust. J. Chem. **60**, 484 (2007).
22. M. Gu, *Advanced Optical Imaging Theory* (Springer, 2000).
23. J. Serbin, A. Egbert, A. Ostendorf, B. N. Chichkov, R. Houbertz, G. Domann, J. Schulz, C. Cronauer, L. Frhlich, and M. Popall, Opt. Lett. **28**, 301 (2003).
24. S. G. Johnson and J. D. Joannopoulos, MIT Photonic Bands Software, http://ab-initio.mit.edu/mpb.